Rheol Acta (2017) 56:765–778
DOI 10.1007/s00397-017-1031-2

ORIGINAL CONTRIBUTION

The interface migration in shear-banded micellar solutions

Juan Paulo Garcia-Sandoval[1] · Fernando Bautista[1] · Jorge Emilio Puig[1] · Octavio Manero[2]

Received: 6 March 2017 / Revised: 26 July 2017 / Accepted: 26 July 2017 / Published online: 11 August 2017

Abstract In this work, we study the diffusion of the interface between bands in wormlike micellar solutions that exhibit shear banding flow regimes, namely, systems undergoing coexistence of states of different shear rates along a constant stress plateau. The migration of the interface between bands possessing different birefringence levels is predicted by the BMP (Bautista-Manero-Puig) model in which a structural parameter (the fluidity) presents two states with differing order separated by an interface. The mechanical potential derived from the constitutive equations and a diffusion term for the structure evolution equation predict various time scales of interface migration at the inception of shear flow and under shear-rate changes along the plateau stress. It is shown that the extremes of the plateau (binodals) correspond to the minima in the mechanical potential as a function of fluidity or shear rate. We also predict the dependence of the diffusive length scale on the applied shear rate.

Keywords Phase field method · BMP model · Interface migration · Micellar solutions

✉ Octavio Manero
manero@unam.mx

[1] Departamentos de Ingeniería Química y Física, Universidad de Guadalajara, Blvd. M. García Barragán 1451, Guadalajara, Jal., 44430, México

[2] Instituto de Investigaciones en Materiales, Universidad Nacional Autónoma de México, Ciudad Universitaria, Ciudad de México, 04510, México

Introduction

Wormlike micellar solutions under shear flow often exhibit a plateau stress that is independent on fluid history along moderate shear rates, inducing the formation of shear bands of different optical and rheological properties. The description of this flow behavior involves a cubic equation of state, which in analogy with the van-der-Waals theory of phase separation or gradient theory of gas-liquid interface (Van der Waals 1895), undergoes spinodal decomposition to produce two stable states with different order. The macroscopic order-parameter is usually the micellar stress in the constitutive equations, and the diffusion mechanism of the interface between bands would naturally involve a phase-field or order parameter related with the current stress. However, if birefringence bands prediction is sought, alternative order parameters can be suggested, such as a parameter representing the fluid structure as in the present study.

Elsewhere (Castillo et al. 2014), we have analyzed the mechanical potential derived from a constitutive equation representing the internal structure of the fluid coupled to an invariant rheological equation for the stress (the generalized BMP model, Manero et al. 2007). It has been shown that the mechanical potential inherent in the BMP model is similar to the Ginzburg-Landau (G-L) model for thermodynamic first-order phase transitions (Frank et al. 2012). In fact, the mechanical potential has two minima of equal depth that signals the "binodals" or extremes of the plateau stress. In the construction of the potential, an "order parameter" is defined, namely, the modified fluidity, which is itself the structure variable. Bifurcation parameters are also defined, in such a way that for conditions where an interface is formed, they determine the locus of the stress plateau

and hence the minima of the potential. This potential resembles the free energy associated with the interface in the G-L equation.

Hu and Lips (2005), Hu et al. (2008) produced a flow curve from local stress and shear rate obtained from measured velocity profiles in a micellar solution made of cetylpyridinium chloride and sodium salicylate. Emphasis is made on the difference between shear-thinning and shear banding, although both regimes may show non-linear velocity profiles. For concentrations larger than 4.9 wt. %, large jumps in the local shear rate at the interface reveal the existence of an underlying non-monotonic flow curve, where two stages of temporary banding and permanent banding occur. Temporary banding manifests abruptly just after the large overshoot observed at the inception of flow and before the undershoot appearing past the maximum, corresponding to the region where the stress becomes multivalued and the system becomes unstable. For longer times after the stress undershoot, permanent banding sets in; steady shear banding is observed only in a solution with a non-monotonic constitutive curve. A distinctive feature of shear banding flow is the induction time observed under imposed controlled stress. The shear rate presents two steps as a function of time: before the induction period, the velocity profile remains linear, but after that the profile becomes banded; hence the induction time is consistent with the existence of a metastable state.

López-Barrón et al. (2014) analyzed the microstructure of a similar micellar solution employed by Hu et al. at the inception of shear flow and under stress relaxation. After an initial elastic response at the inception of flow, shear banding kinematics within a metastable regime of nearly homogeneous flow follows. Past six relaxation times, the onset for shear banding occurs. The butterfly patterns in light scattering reveal shear-induced concentration fluctuations. During flow startup and after the initial stress overshoot, the solution is flow-aligned and disentangled, corresponding to a microstructure consistent with the high shear-rate band of the underlying constitutive curve, whereas the evolving low-shear band has a microstructure consistent with the low-shear branch of the constitutive equation (entangled). Following the abrupt drop in viscosity, the homogeneous metastable fluid is flow aligned and corresponds to the high shear-rate branch, with butterfly patterns that signal the flow-induced heterogeneities on the micron length scale. The two stages of stress relaxation have been assigned to large density fluctuations at short times followed by a relaxation of micelle orientation. These two stages of stress relaxation have been observed and predicted by the BMP model (see Soltero et al. 1999).

Helgeson et al. (2009) used a solution of CTAB near the isotropic-nematic thermodynamic transition, which presents a non-Maxwellian behavior. Results suggest that shear banding in these micellar solutions is connected to the underlying non-equilibrium phase transition behavior. The location of the interface between the high-shear band and the low-shear band is defined by the location where the local shear rate exhibits a discontinuity, shown by the sudden change of slope of the velocity profiles as functions of radial distance. A linear relationship between the interface location along the flow cell and shear rate is obtained along the stress plateau; hence the linear lever rule applies here. Moreover, SANS data (orientation angle, alignment factor and flow birefringence) indicate that the structure changes smoothly along the flow cell, as opposed to the abrupt variation of the shear rate. With similar methodology with respect to velocity profiles, Ballesta et al. (2007) used small amplitude oscillatory shear superimposed to steady shear in the shear banding regime, measuring the velocity profiles to yield the interface position as a function of time in the flow cell. An exponential change of the interface position with time is revealed. Among the papers dealing with the variation of the interface width with shear rate or imposed pressure gradient, Masselon et al. (2008) studied the flow of semi-dilute wormlike micellar solution in a straight microchannel by particle image velocimetry. The correlation length or interface width was estimated using a non-local diffusive model. This work is one among the few that predicts a variable interfacial width with shear rate in the plateau region of the stress as the applied pressure gradient increases. Fardin et al. (2015) measured the position of the interface as a function of time and found an exponential change for various applied shear rates during the interface migration time. From each of the curves, a characteristic migration time is extracted, which was found to increase mono-exponentially with applied shear rate. Models by Giesekus and Johnson-Segalman do not predict these experiments, since the migration time does not follow an exponential increase, but a linear or slower one, which implies a single value of the interfacial width.

In summary, the interface generation between shear bands following start-up of shear flow comprises a stage of migration (Radulescu et al. 2003; Fardin et al. 2015). The building of the banding structure starts with the relaxation of the stress overshoot, accompanied with the formation of a diffusive interface that migrates from the fixed wall to its stationary position in the gap. The migration is performed first rapidly and thereafter more slowly. This process is accompanied with sharpening of the interface, the profile of which is initially flat along the vorticity direction. The interface continues to move up to the equilibrium position associated with the plateau value. Yuan (1999) describes the dynamics of the mechanical interface in wormlike micelles using the diffusive model of Johnson and Segalman (1977). It is shown that the transit period during interface

migration can be much longer than the stress relaxation time.

Several models have been proposed to account for the time scales of interface diffusion (Radulescu et al. 2003). Therein, the front propagation toward the final equilibrium position is controlled by the stress diffusion. Recently, Fardin et al. (2015) reported diffusive length scales of the order of few micrometers, revealing that this length scale is a strong function of the applied shear rate, decreasing rapidly across the stress plateau. Calculations using several constitutive equations cannot predict this behavior, and argumentation is given on the issue of incorporating the dependence of the diffusive length scale on the applied shear rate.

In this work, we consider the BMP mechanical potential to describe the interface dynamics and properties of systems of wormlike micelles under simple shear flow. Using this formulation, it is then possible to describe the interfacial width. For a given control variable, shear stress or shear rate, the depth and position of the minima in the potential can be calculated, from which the interface dynamics can be described. The constitutive equation generates as a special case, the G-L equation that describes the interface diffusion in terms of the BMP model parameters. This equation is a reaction-diffusion equation that allows asymptotic solutions for a small diffusion coefficient. It is shown that the fluidity tends rapidly to a minimum in the mechanical potential, and when this potential has several minima, it tends to a piecewise constant function. Each interface is found to move along its normal with a constant velocity determined by the discontinuity in the mechanical potential across the interface.

This work aims to predict the birefringence data of a moving interface, where a region of ordered fluid coexists with a more disordered region, separated by a moving interface, set in motion by step changes in the shear rate, at the inception of flow and along the stress plateau. For this sake, the order parameter is here the normalized fluidity. One of the objectives of this work is to explicitly formulate the shear rate dependence of the diffusion length which has not been predicted by other models, such as the diffusive Johnson-Segalman and Giesekus ones. Experiments also support that a structure-dependent relaxation time is necessary (Fardin et al. 2015). For this purpose, the dependence of the stress relaxation time on the system structure, contained in the BMP constitutive equation, allows the description of an interface width that varies with shear rate.

Constitutive equations

The set of equations of the generalized BMP model (Manero et al. 2007) are here expressed by the evolution equations of the structure parameter (φ/φ_0) and the relaxation equation for the stress $\underline{\underline{\sigma}}$. These equations read:

$$\frac{d\varphi}{dt} = k_0\left(1+\vartheta\left(\sqrt{II_D}\right)\right)(\varphi_\infty-\varphi)\,\underline{\underline{\sigma}}:\underline{\underline{D}} + \frac{1}{\lambda}(\varphi_0-\varphi)+\kappa_\varphi\nabla^2\varphi \tag{1}$$

$$\underline{\underline{\sigma}}+\lambda_\sigma(\varphi)\overset{\triangledown}{\underline{\underline{\sigma}}} = \frac{2}{\varphi}\underline{\underline{D}} \tag{2}$$

where $\underline{\underline{D}}$ is the symmetric part of the velocity gradient tensor $\underline{\underline{L}}$. The shear banding intensity parameter, ϑ, is a function of II_D, the second invariant of $\mathbf{D}$ (namely, the shear rate) representing the cubic non-linearity of the constitutive curve related to the minima of the potential and to the span of the plateau stress. φ, the inverse of the shear viscosity (η) is the fluidity $\varphi_0(\equiv\eta_0^{-1})$ is the fluidity at zero shear rate, φ_∞ is the fluidity at high shear rates, λ_σ is the stress relaxation time that is function of fluidity, λ is a structure relaxation time, k_0 is a kinetic parameter for structure breaking. κ_φ is a diffusion coefficient and the upper-convected derivative of the stress tensor $\underline{\underline{\sigma}}$ is defined as:

$$\overset{\triangledown}{\underline{\underline{\sigma}}} = \frac{d\underline{\underline{\sigma}}}{dt} - \left(\underline{\underline{L}}\cdot\underline{\underline{\sigma}}+\underline{\underline{\sigma}}\cdot\underline{\underline{L}}^T\right). \tag{3}$$

Notice that the stress relaxation time in Eq. 2, $\lambda_\sigma(\varphi)$ is a variable that depends on the structure represented by the local fluidity that evolves according to Eq. 1. For slow flows, $\lambda_\sigma(\varphi_0)$ is the Maxwell relaxation time, and the limit for strong flows is $\lambda_\sigma(\varphi_\infty)$.

The mechanical potential of the BMP constitutive equation

Under simple-shear flow, the shear rate is given by $\partial v_x/\partial y$ (x is the flow direction, y is that of the velocity gradient and z is the direction of the vorticity), Eqs. 1 and 2 become:

$$\frac{d\varphi}{dt} = k_0\left(1+\vartheta\frac{\partial v_x}{\partial y}\right)(\varphi_\infty-\varphi)\,\sigma_{xy}\frac{\partial v_x}{\partial y} + \frac{1}{\lambda}(\varphi_0-\varphi)+\kappa_\varphi\frac{\partial^2\varphi}{\partial y^2} \tag{4}$$

$$\sigma_{xy}+\lambda_\sigma(\varphi)\left[\frac{\partial\sigma_{xy}}{\partial t}-\frac{\partial v_x}{\partial y}\sigma_{yy}\right] = \frac{1}{\varphi}\frac{\partial v_x}{\partial y} \tag{5}$$

$$\sigma_{xx}+\lambda_\sigma(\varphi)\left[\frac{\partial\sigma_{xx}}{\partial t}-2\frac{\partial v_x}{\partial y}\sigma_{xy}\right] = 0 \tag{6}$$

$$\sigma_{ii}+\frac{1}{G_0\varphi}\left[\frac{\partial\sigma_{ii}}{\partial t}\right] = 0,\ i=y,z \tag{7}$$

Small inertia in the stress equation has been considered. The following conservation equations hold:

$$\frac{\partial v_x}{\partial x} = 0, \tag{8}$$

$$\rho \frac{\partial v_x}{\partial t} = \frac{\partial \sigma_{xy}}{\partial y} + \eta_s \frac{\partial^2 v_x}{\partial y^2}. \tag{9}$$

η_s is the solvent viscosity. Under homogeneous steady-state flow, from Eqs. 4, 5, and 7, we obtain:

$$0 = \frac{1}{\lambda}(\varphi_0 - \varphi) + k_0 \left(1 + \vartheta \sigma_{xy} \varphi\right)(\varphi_\infty - \varphi)\sigma_{xy}^2 \varphi \tag{10}$$

This is a cubic equation in φ, which may be expressed as:

$$\varphi^3 - a\varphi^2 + b\varphi - c = 0 \tag{11}$$

where

$$a = \varphi_\infty - \frac{1}{\vartheta \sigma_{xy}}, \quad b = \frac{\frac{1}{k_0 \lambda \sigma_{xy}^2} - \varphi_\infty}{\vartheta \sigma_{xy}} \quad \text{and}$$

$$c = \frac{\varphi_0}{k_0 \lambda \vartheta \sigma_{xy}^3}. \tag{12}$$

Defining the modified fluidity as:

$$\varphi^o = \varphi - a/3, \tag{13}$$

Equation 11 becomes:

$$\left(\varphi^o\right)^3 - u\varphi^o + v = 0, \tag{14}$$

where

$$u = a^2/3 - b \quad \text{and} \quad v = ab/3 - 2a^3/27 - c. \tag{15}$$

The integral of Eq. 14 gives the BMP mechanical potential:

$$V = \frac{1}{4}\left(\varphi^o\right)^4 - \frac{u}{2}\left(\varphi^o\right)^2 + v\varphi^o. \tag{16}$$

If $v = 0$, the potential is symmetric, and Eq. 14 gives the following solutions:

$$\varphi_1^o = \sqrt{u}, \quad \varphi_2^o = -\sqrt{u}, \quad \varphi_3^o = 0. \tag{17}$$

Substituting the roots given in Eq. 17 in Eq. 16, the value of the minima of the potential is obtained (located at the values given in Eq. 17):

$$V = -u^2/4. \tag{18}$$

The Ginzburg-Landau or Allen-Cahn equation

The G-L equation governs the evolution of an order parameter which denotes a field whose values describe the phase of the system under consideration. To obtain it from the BMP equations, we assume that the stress relaxes in a time scale shorter that of the structure; such assumption agrees with the predictions by Yuan (1999) and with experiments of Hu et al. (2008) and López-Barrón et al. (2014). In this regard, the equation for the structure and the relaxed stress equations are:

$$\frac{d\varphi}{dt} = k_0 \left(1 + \vartheta \frac{\partial v_x}{\partial y}\right)(\varphi_\infty - \varphi)\sigma_{xy} \frac{\partial v_x}{\partial y} + \frac{1}{\lambda}(\varphi_0 - \varphi) + \kappa_\varphi \frac{\partial^2 \varphi}{\partial y^2} \quad \text{(4 revisited)}$$

$$\sigma_{xy} = \frac{1}{\varphi}\frac{\partial v_x}{\partial y} \tag{19}$$

Upon substituting the relaxed stress (19) into Eq. 4, we obtain:

$$\frac{1}{k_0 \vartheta \sigma_{xy}^3}\frac{d\varphi}{dt} = \frac{\varphi_0}{k_0 \lambda \vartheta \sigma_{xy}^3} - \left(\frac{1}{k_0 \lambda \vartheta \sigma_{xy}^3} - \frac{\varphi_\infty}{\vartheta \sigma_{xy}}\right)\varphi - \left(\frac{1}{\vartheta \sigma_{xy}} - \varphi_\infty\right)\varphi^2 - \varphi^3 + \frac{\kappa_\varphi}{k_0 \vartheta \sigma_{xy}^3}\frac{\partial^2 \varphi}{\partial y^2} \tag{20}$$

Or, alternatively,

$$\frac{1}{k_0 \vartheta \sigma_{xy}^3}\frac{d\varphi}{dt} = c - b\varphi + a\varphi^2 - \varphi^3 + \frac{\kappa_\varphi}{k_0 \vartheta \sigma_{xy}^3}\frac{\partial^2 \varphi}{\partial y^2} \tag{21}$$

where a, b, and c are given in Eq. 12.

In terms of the modified fluidity (as defined in Eq. 13), Eq. 21 becomes:

$$\frac{1}{k_0 \vartheta \sigma_{xy}^3}\frac{d\varphi^o}{dt} = -v + u\varphi^o - \left(\varphi^o\right)^3 + \frac{\kappa_\varphi}{k_0 \vartheta \sigma_{xy}^3}\frac{\partial^2 \varphi^o}{\partial y^2} \tag{22}$$

where u and v are given in Eq. 15. If $v = 0$, upon defining the following relations: $\varepsilon = \frac{1}{k_0 \vartheta \sigma_{xy}^3}$ and $V'(\varphi^o) = \frac{\partial V}{\partial \varphi^o}$, Eq. 22 becomes:

$$\varepsilon \frac{d\varphi^o}{dt} = -V'\left(\varphi^o\right) + \kappa_\varphi \varepsilon \frac{\partial^2 \varphi^o}{\partial y^2} \tag{23}$$

In the particular case where κ_φ is of order ε, and ε is a small parameter, we seek solutions to the following reaction-diffusion equation:

$$\varepsilon \frac{d\varphi^o}{dt} = -V'\left(\varphi^o\right) + \varepsilon^2 \frac{\partial^2 \varphi^o}{\partial y^2} \tag{24}$$

In fact, under homogeneous steady-state, $V' = 0$ and we recover Eq. 14 with $v = 0$. We seek the asymptotic behavior of φ^0 as $\varepsilon \to 0$. We also assume that the initial and boundary conditions are satisfied:

$$\varphi^o(y, 0) = \varphi_1^o, \ y < y_i \ \text{(interface)}; \ \varphi^o(y, 0) = \varphi_2^o, \ y > y_i \tag{25}$$

$$d\varphi^o/dy = 0, \ y \pm \infty \tag{26}$$

where the derivative is normal to the interface. Three time scales are here considered. The *shortest time scale* derives from Eq. 24 as the diffusive term goes to zero:

$$\frac{d\varphi^o}{dt} = -\varepsilon^{-1} V'\left(\varphi^o\right). \tag{27}$$

The solution of Eq. 27 is

$$\varphi^o\left(y,t\right) = \varphi_1^o,\ \ y < y_i\ \ \text{(interface)}\,;\ \ \varphi^o\left(y,t\right) = \varphi_2^o,\ \ y > y_i \tag{28}$$

The discontinuity at $y = y_i$ represents a shock and it is a manifestation of the fact that we neglected the diffusion term. If we restore the diffusion term, the discontinuity becomes smooth. Since the second term in Eq. 27 becomes large as $\varepsilon \to 0$, a particular perturbation is suggested:

$$\varphi^o\left(t\right) = \varphi_0^o\left(1 + \delta\left(t\right)\right) \tag{29}$$

Substituting (29) in Eq. 27, to order δ we have:

$$\frac{\partial \delta}{\partial t} = -2u\delta \ \rightarrow\ \delta\left(t\right) = \delta\left(0\right)\exp\left(-2ut\right). \tag{30}$$

The perturbation δ decays exponentially to a steady-state solution $\left(\varphi^o\right)^2 = u$, with $\varphi_1^o = -\sqrt{u}$ and $\varphi_2^o = \sqrt{u}$. This is called *forward pitchfork bifurcation*, which has inversion symmetry with respect to φ^o and the bifurcating solutions must be symmetric about $\varphi^o = 0$. For $u < 0$, there is a single stable point at $\varphi^o = 0$. For $u > 0$ the $\varphi^o = 0$ fixed point remains, but is unstable and two new, stable fixed points φ_1^o and φ_2^o develop.

Convective time scale

In the general case of a moving interface, assuming that the interface speed is $s = dy/dt$ and introducing the stretched variable:

$$\overline{y} = \left(y + st\right)/\varepsilon \tag{31}$$

such as $\varphi^o = \varphi^o\left(y\left(\overline{y}\right),t\right)$, the material time derivative can be expressed as:

$$\begin{aligned}\frac{d\varphi^o}{dt} &= \frac{\partial\varphi^o}{\partial t} + \frac{\partial\varphi^o}{\partial y}\frac{dy}{dt} = \frac{\partial\varphi^o}{\partial t} + \frac{\partial\varphi^o}{\partial\overline{y}}\frac{\partial\overline{y}}{\partial y}\frac{dy}{dt}\\ &= \frac{\partial\varphi^o}{\partial t} + \frac{s}{\varepsilon}\frac{\partial\varphi^o}{\partial\overline{y}}\end{aligned} \tag{32}$$

Equation 22 becomes:

$$\frac{\partial\varphi^o}{\partial t} + \frac{s}{\varepsilon}\frac{\partial\varphi^o}{\partial\overline{y}} + \frac{1}{\varepsilon}\frac{\partial V}{\partial\varphi^o} = \frac{1}{\varepsilon}\frac{\partial^2\varphi^o}{\partial\overline{y}^2} \tag{33}$$

The leading order equation is then:

$$s\frac{\partial\varphi^o}{\partial\overline{y}} + \frac{\partial V}{\partial\varphi^o} = \frac{\partial^2\varphi^o}{\partial\overline{y}^2} \tag{34}$$

with boundary conditions given in Eq. 25. Equation 34 represents a non-linear eigenvalue problem with eigenvalue s. This equation is similar to Newton's equation for an inertial particle in an inverted potential $(-V)$ with a friction term.

Under the convective time scale, that corresponding to negligible diffusion, Eq. 34 can be multiplied by $\partial\varphi^o/\partial\overline{y}$ on both sides and integrate from $y = -\infty$ to $y = +\infty$ to obtain the following relation involving the jump $[V] = V\left(\varphi_1^o\right) - V\left(\varphi_2^o\right)$ across the interface:

$$s = \frac{V\left(\varphi_1\right) - V\left(\varphi_2\right)}{\int\limits_{-\infty}^{+\infty}\left(\partial\varphi/\partial\overline{y}\right)^2 d\overline{y}} \tag{35}$$

At this time scale, the interface moves to the region of lowest free energy, with a constant normal velocity, than depends on the difference in the free energy between the two minima φ_1^o and φ_2^o. When $V\left(\varphi_1^o\right) - V\left(\varphi_2^o\right) = 0$ the interface velocity is zero, which indicates that the front will not move. Then, it justifies the fact that the potential $V\left(\varphi^o\right)$ is symmetric, with two minima located at the positions φ_1^o and φ_2^o (see Eq. 16) and also justifies the condition $v = 0$ in Eq. 16.

Diffusive time scale

The dynamics of the interface at longer time scales can be described by rescaling the problem by replacing t by εt^* in Eq. 24 to obtain:

$$\varepsilon\frac{d\varphi^o}{dt^*} + \frac{1}{\varepsilon}V'\left(\varphi^o\right) = \frac{1}{\varepsilon}\frac{\partial^2\varphi^o}{\partial y^2} \tag{36}$$

The leading order equation now becomes:

$$\kappa_\varphi\frac{\partial^2\varphi^o}{\partial y^2} = \frac{\partial V}{\partial\varphi^o} = \left(\varphi^o\right)^3 - u\varphi^o \tag{37}$$

with boundary condition $\lim_{y\to\pm\infty}\varphi^o = \pm\sqrt{u}$, and in which we have introduced the constant diffusion coefficient. The solution of Eq. 37 is:

$$\varphi^o\left(y\right) = \pm\sqrt{u}\tanh\left(\frac{y}{\sqrt{2}\xi}\right), \tag{38}$$

where the interface thickness (correlation length) is $\xi = \sqrt{\kappa_\varphi/u}$.

For long times, after the profile has settled down, the spatial integration of Eq. 37 gives

$$V\left(y\right) = \kappa_\varphi\frac{\partial\varphi^o}{\partial y}. \tag{39}$$

Equation 39 expresses the spatial variation of the mechanical potential. To obtain Eq. 39, use has been made of the following linear relation: $d\varphi^o = \frac{\partial\varphi^o}{\partial y}dy$.

Summarizing, when $[V] = 0$, the interface has velocity zero. Equation 24 can be written as a gradient flow in space in the form:

$$\frac{\partial\varphi^o}{\partial t} = -\frac{\delta F\left(\varphi^o\right)}{\delta\varphi^o} \tag{40}$$

Here, the functional $F(\varphi^o)$ is defined as:

$$F\left[\varphi^o\right] = \int_{\Omega} \left\{ \frac{1}{\varepsilon} V\left(\varphi^o\left(\underline{x}\right)\right) + \frac{1}{2}\varepsilon \left|\nabla\varphi^o\left(\underline{\underline{x}}\right)\right|^2 \right\} d\underline{x} \qquad (41)$$

Equation 40 expresses that φ^o moves in the direction of decreasing F, so it tends to a stable local minimizer of F. In this regard, when V has two minimizers φ_1^o and φ_2^o with $V\left(\varphi_1^o\right) = V\left(\varphi_2^o\right)$, any local minimizer converges as $\varepsilon \to 0$, to a piecewise constant function φ_C^o with values φ_1^o and φ_2^o. Furthermore, the interfaces across which φ_C jumps are local minimizers of surface area.

When the solution $\varphi^o(y,t)$ of the gradient flow, Eq. 40, converges to φ_C^o, the solution of the gradient flow is:

$$\frac{\partial\varphi_C^o}{\partial t} = -\frac{\delta F\left(\varphi_C^o\right)}{\delta\varphi_C^o}. \qquad (42)$$

Variable diffusion length

The coefficient of the diffusion term in Eq. 38 may be shear-rate dependent. In our case, a dependence on the fluid structure is suggested, in such a way that

$$\kappa_\varphi(\varphi) = D'\lambda_\sigma(\varphi) \qquad (43)$$

where D' is a diffusion constant and the relaxation time is function of the structure represented by the fluidity. According to Eq. 43, the interface width corresponding to Eq. 38 is

$$\xi = \sqrt{\frac{\kappa_\varphi}{u/\varphi_\infty^2}} = \sqrt{\frac{\varphi_\infty^2 D'\lambda_\sigma(\varphi)}{u}} \qquad (44)$$

where u has been normalized with respect to the maximum fluidity. The proportionality implied in Eq. 44, $\xi \sim \lambda_\sigma^{1/2}(\varphi)$, is a new result. In fact, if the fluidity increases as the shear rate increases along the plateau stress (around 2 decades, as normally observed in micellar systems), and $\lambda_\sigma(\varphi)$ is a decreasing function of fluidity, for instance $\lambda_\sigma(\varphi) = \lambda_{\sigma 0}/\varphi$, the interface width should decrease one decade. This proportionality is shared with experiments reported recently (Fardin et al. 2015).

Methodology

Two set of experimental data of a wormlike micellar solutions were used (experiments were not conducted in this investigation). The first one, is a 5 wt. % CTAT wormlike micellar solution at 38 °C whose BMP parameters were reported in a recent study (Castillo et al. 2014): $\varphi_0 = 0.069\ (\text{Pa}\cdot\text{s})^{-1}$, $\varphi_\infty = 10\ (\text{Pa}\cdot\text{s})^{-1}$, $k_0\lambda = 5\times10^{-5}$ s/Pa, $\vartheta = 0.012$ s, $\lambda_\sigma = 1/G_0\varphi$ s, $G_0 = 57.5$ Pa and $\lambda = 0.05 G_0\varphi_0$ s, $\rho = 1000\ \text{kg}\cdot\text{m}^{-3}$, $\eta_s = 0.001$ Pa · s and $l = 0.02$ m, while the the second one, a 11 wt. % CTAB-$NaNO_3$ wormlike micellar solution at 28 °C, was used to compare the predictions of our model with the experimental data of Fardin et al. (2015). For this solution, the BMP model was fitted using a the Nelder-Mead simplex algorithm as described in Lagarias et al. (1998), obtaining the following parameters: $\varphi_0 = 3.03\times10^{-3}\ (\text{Pa}\cdot\text{s})^{-1}$, $\varphi_\infty = 0.909\ (\text{Pa}\cdot\text{s})^{-1}$, $k_0\lambda = 9.14\times10^{-6}\ \text{s}\cdot\text{Pa}^{-1}$, $\vartheta = 0.135$ s, $\lambda_\sigma = \lambda_{\sigma 0}(1-\varphi/\varphi_\infty)/(1-\varphi/\varphi_\sigma)$ s, $\lambda_{\sigma 0} = 0.168$ s, $\varphi_\sigma = 1.01\ (\text{Pa}\cdot\text{s})^{-1}$ and $\lambda = 0.1\lambda_{\sigma 0}$ s, $\rho = 1000\,\text{kg}\cdot\text{m}^{-3}$, $\eta_s = 0.001$ Pa · s and $l = 0.002$ m (all quantities in international units).

Equations 4–6 and 9 were solved using a partial discretization method: first the spatial derivatives were approximated using central finite differences to transform the system into a set of ordinary differential equations that were solved using an implementation of TR-BDF2, an implicit Runge-Kutta formula with a first stage that is a trapezoidal rule step and a second stage that is a backward differentiation formula of order two (Hosea and Shampine 1996). The interface migration was studied by analyzing the spatial gradient of both the potential function and the velocity profile.

Results

Figures 1, 2, 3, 4, 5, 6, and 10b present results using the parameters for the 5 wt. % CTAT wormlike micellar solution at 38 °C, while Figs. 7, 8, 9 and 10a present results using the parameters for the 11 wt. % CTAB-$NaNO_3$ wormlike micellar solution at 28 °C.

The mechanical potential shows two minima of equal magnitude, symmetrically distributed around $\varphi_3^o = 0$, where the maximum is located. The well of the potential and span of the minima are solely functions of the parameter u. For an imposed shear stress σ_{xy}, the parameters a, b, and c (12) can be calculated, from which the bifurcation parameters u and v can also be evaluated (15). There is a value of the stress (plateau stress) at which $v = 0$, determining a u-value that signals the position of the minima and depth of the potential (see Figs. 1 and 2), and therefore, the two minima define the position of the plateau stress. It is important to mention that along the plateau the stress is constant, and hence u is also constant. A *unique mechanical spectrum* $V(\varphi^o)$ is generated along the plateau stress, and therefore, the depth of the potential and the location of the minima are henceforth equal at the extremes of the plateau (see Fig. 2). This is a fully mechanical spectrum whose minima do not need a thermodynamic potential or free energy to be specified.

Solution of Eqs. 4–6 gives the constitutive flow curve (stress versus shear rate, $\sigma(\dot\gamma)$), the potential, fluidity and modified fluidity as a function of shear rate defined as:

$$\frac{1}{l}\int_0^l \frac{\partial v_x(y,t)}{\partial y} dy = \dot\gamma, \qquad (45)$$

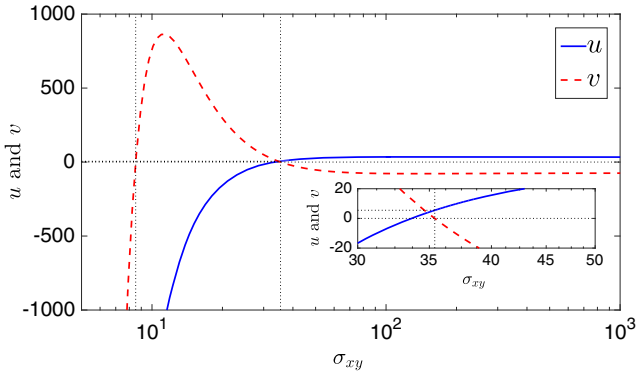

Fig. 1 Bifurcation parameters u and v as functions of the applied stress for a 5 wt. % CTAT wormlike micellar solution at 38 °C. Inset: Amplified view which indicates the u-value corresponding to $v = 0$. Notice that as $v = 0$, there is a u-value that determines de plateau stress

where l is the distance between the parallel plates of the flow cell. In Fig. 3a–c the mechanical spectrum, stress, fluidity and modified fluidity are shown as functions of shear rate. Notice that the mechanical spectrum as a function of shear

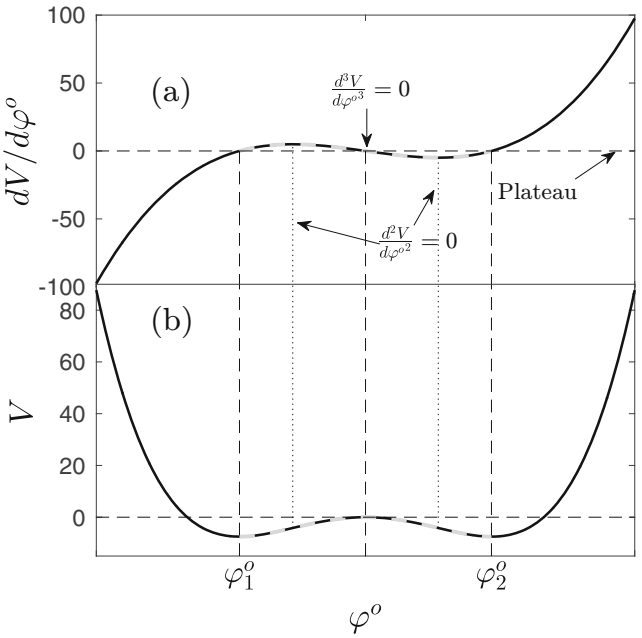

Fig. 2 The mechanical potential and its derivative as functions of modified fluidity for a 5 wt. % CTAT wormlike micellar solution at 38 °C. Notice that the potential is symmetric, and the two minima define de extremes of the plateau stress. The two minima are located at values of the modified fluidity given in Eq. 17, and the potential depth is given in Eq. 18. Notice that this construction requires a constant value of u, which is only achieved along the plateau stress. The roots of $V\ (\varphi^o)$ are $\left(-\sqrt{2u}, 0, \sqrt{2u}\right)$. The first derivatives (maximum and minima) are located at $\left(-\sqrt{u}, 0, \sqrt{u}\right)$, which coincide with the extremes of the plateau. The second derivative (inflection points) are located at $\left(-\sqrt{u/3}, 0, \sqrt{u/3}\right)$ and the third derivative signals the maximum located at $\varphi^o = 0$

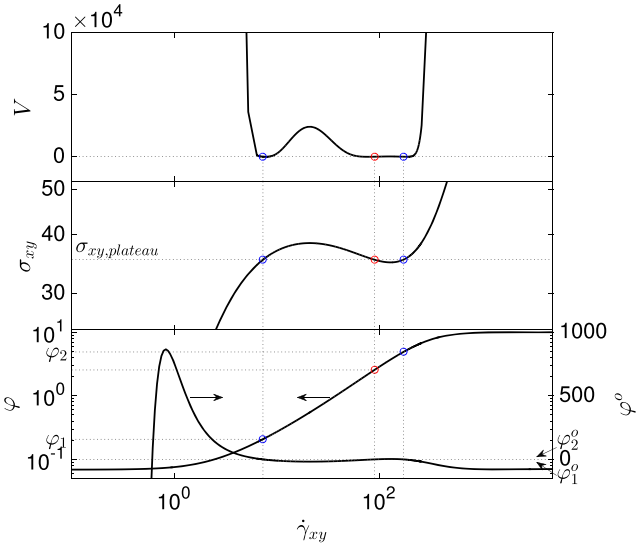

Fig. 3 The mechanical potential (**a**), stress (**b**), fluidity and modified fluidity (**c**) as functions of shear rate for a 5 wt. % CTAT wormlike micellar solution at 38 °C. Notice that the minima shown in Fig. 3a coincide with the minima of the potential in Fig. 2. Concurrently, the extremes of the plateau stress in **b** coincide with those in Fig. 2. Because the scale shown in **c**, the values of the modified fluidity at the extremes of the plateau $\left(-\sqrt{u}, \sqrt{u}\right)$ are difficult to observe

rate possesses two minima located at the critical shear rates $\dot{\gamma}_1$ and $\dot{\gamma}_2$ (extremes of the plateau) similarly to the minima in the $V\ (\varphi^o)$ spectrum (see Fig. 3a). There is another minimum located at the inflection point of the $\sigma\ (\dot{\gamma})$ curve (Fig. 3b) corresponding to $\varphi^o = 0$ (Fig. 3c). Therefore, the plateau stress is univocally determined in the $V\ (\varphi^o)$ and $V\ (\dot{\gamma})$ spectra. Indeed, at the extremes of the plateau (binodals), the relation between shear rate $(\dot{\gamma})$ and modified fluidity (φ^o) is $\dot{\gamma} = \sigma_p\ (\varphi^o + a/3)$. For a constant stress σ_p, $d\dot{\gamma} = \sigma_p d\varphi^o$, hence $\partial V/\partial\dot{\gamma} = \sigma_p^{-1}\partial V/\partial\varphi^o$, and thus the minima located at φ_1^o and φ_2^o coincide with the locus of the critical shear rates $\dot{\gamma}_1$ and $\dot{\gamma}_2$.

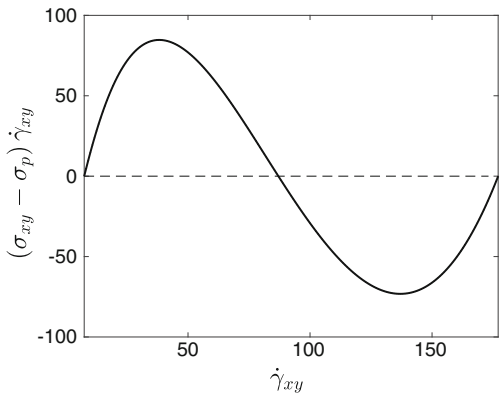

Fig. 4 Dissipation as a function of shear rate for a 5 wt. % CTAT wormlike micellar solution at 38 °C. Dashed line signals the equal area line

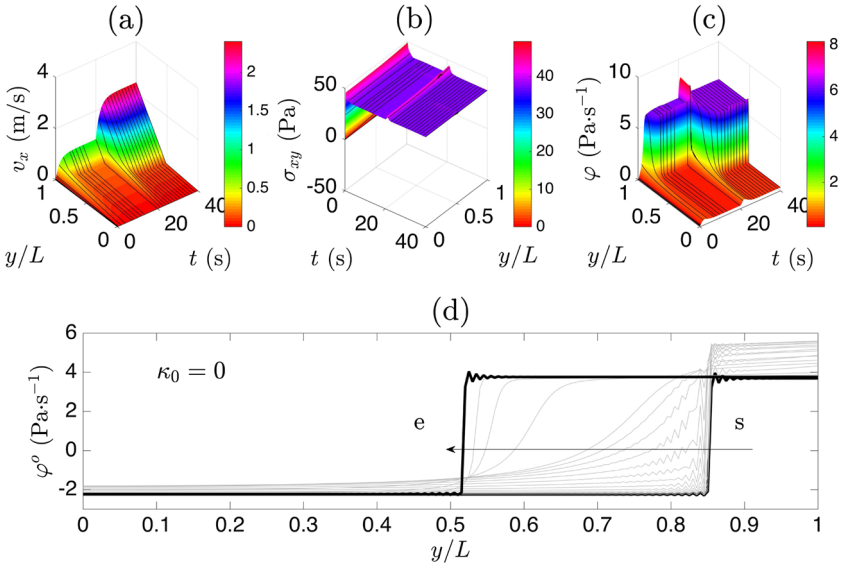

Fig. 5 Convective time scale. **a** Velocity profiles, **b** polymeric stress, **c** fluidity and **d** interface migration as functions of space and time for a 5 wt. % CTAT wormlike micellar solution at 38 °C. Two-stage step-shear: 0 - 44s^{-1} and 44-120 s^{-1} (between two banded states). s and e denote the start and end of the interface migration

Momentum conservation and the equal-area rule

Under steady-state, the momentum conservation (9) yields:

$$\frac{\partial}{\partial y}\left(\sigma\left(\dot{\gamma}\right)+\eta_s\frac{\partial v_x}{\partial y}\right)=0 \tag{46}$$

The constitutive flow curve $\sigma\left(\dot{\gamma}\right)$ and the solvent contribution lead to:

$$\sigma\left(\dot{\gamma}\right)+\eta_s\frac{\partial v_x}{\partial y}=\Sigma \tag{47}$$

where the total stress Σ is independent of y. To meet the requirement that the free energy should be dissipated (i.e., calculating dF/dt), we consider an interface between a low and high shear rate regions. Integration of Eq. 47 yields:

$$0=\int_{\dot{\gamma}_1}^{\dot{\gamma}_2}\left(\sigma\left(\dot{\gamma}\right)+\eta_s\frac{\partial v_x}{\partial y}-\Sigma\right)d\dot{\gamma}. \tag{48}$$

Any inhomogeneity or diffusive contribution to the interface vanishes since in the low and high shear rate phases (extremes of the plateau) the stress is constant, independent of y. Equation 48 implies stress selection by a Maxwell equal area construction in the stress versus shear rate plane, since:

$$\int_{\dot{\gamma}_1}^{\dot{\gamma}_2}\left(\sigma\left(\dot{\gamma}\right)+\eta_s\frac{\partial v_x}{\partial y}\right)d\dot{\gamma}=\Sigma\left(\dot{\gamma}_2-\dot{\gamma}_1\right). \tag{49}$$

Consequently, $\Sigma=\text{kernel}\left(\dot{\gamma}_2\right)=\text{kernel}\left(\dot{\gamma}_1\right)$. In Fig. 4, the equal-area construction is shown by plotting the dissipation

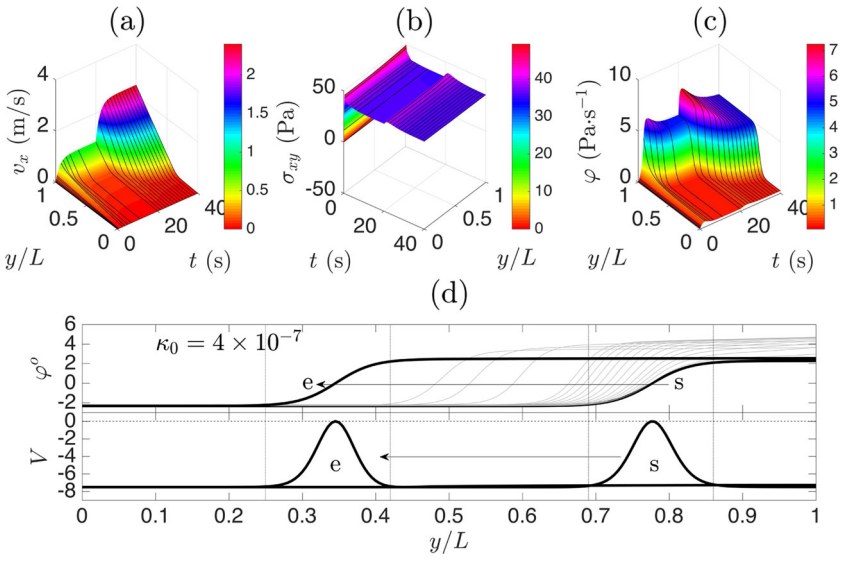

Fig. 6 Diffusive time scale. **a** Velocity profiles, **b** polymeric stress, **c** fluidity, as functions of space and time and (d) interface migration for a 5 wt. % CTAT wormlike micellar solution at 38 °C. The spatial variation of the mechanical potential is shown at the initial and end stages of the interface migration. Two-stage step-shear: 0 - 44s^{-1} and 44-120 s^{-1} (between two banded states). s and e denote the start and end of the interface migration

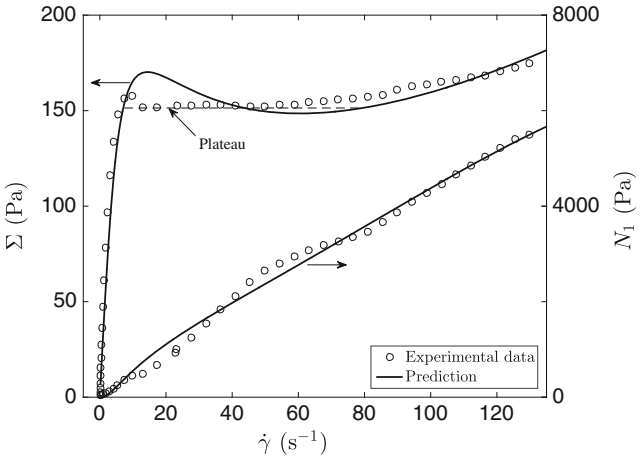

Fig. 7 Shear and normal stress predictions of the BMP model for a 11 wt. % CTAB-$NaNO_3$ wormlike micellar solution at 28 °C (Fardin et al. 2015)

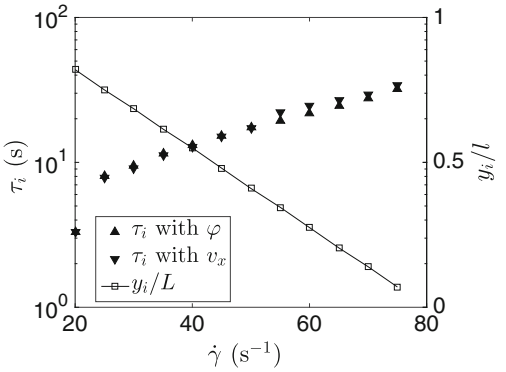

Fig. 9 Migration time of the interface and interface position as a function of applied shear rate for a 11 wt. % CTAB-$NaNO_3$ wormlike micellar solution at 28 °C. The migration time was predicted from the fluidity profile and from the time of formation of the discontinuous velocity profile

versus shear rate. The areas above and below the plateau are equal, validating the equal-areas criterion based on the mechanical potential.

Mechanism for inception of banding instability

This mechanism pertains to a bifurcation point reached as the stress increases along the homogeneous constitutive curve. Upon defining a bifurcation parameter $R = -(u/3)^3 + (v/2)^2$ (where u and v are defined in Eqs. 15), a bifurcation point is reached if $R = 0$. By observing Fig. 1, before the intersection point of v and u, u becomes positive. As the stress is increased, u and v come to a point where the sum of their contributions fulfill the condition $R = 0$. This condition signals the beginning of the flow region where the stress is multivalued and corresponds to the stress reaching, simultaneously, that of the minimum of the flow curve and a point located along the positive slope at low shear rates (see Figs. 2 and 3). At this point, the so-called *Pitchfork*

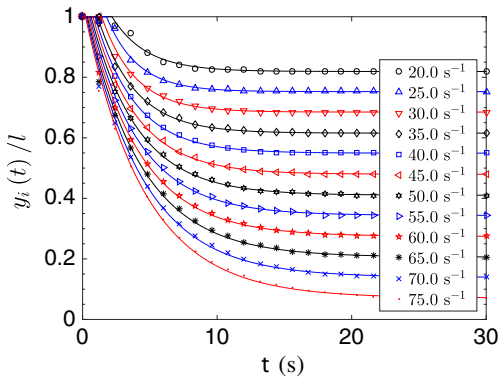

Fig. 8 Interface position as a function of time for various step shear rates from rest to the indicated shear rates for a 11 wt. % CTAB-$NaNO_3$ wormlike micellar solution at 28 °C

bifurcation sets in, and the system becomes unstable. From this point up to the stress maximum (metastable region), a transient shear banding may occur, since the system oscillates between two attractors (see kinetics of shear banding in García-Sandoval et al. 2012). The first attractor is located at the first minimum in V, whereas the second attractor is located at the second minimum. For increasing values of the stress, the condition $v = 0$ is fulfilled and the corresponding value of u signals the position of the stress plateau. For decreasing shear rate starting on the high-shear branch of the flow curve, the process is the same, except that the bifurcation point includes now the maximum of the flow curve.

Interface migration

Figures 5 and 6 depict the variation of the velocity profile, polymeric stress, fluidity and interface diffusion as functions of time and distance between plates. Equations 4–6 and 22 were solved at the inception of flow applying a two-step imposed shear rate history: first, protocol A used by Fardin et al. (2015) was employed to jump from rest up to 44 s^{-1} during 20 s and thereafter, protocol B of Fardin et al. (2015) was used to jump from 44 to 120 s^{-1} (along the stress plateau) subjected to the following boundary conditions:

$$[v_x]_{y=1} = v_{x0}(t) = l\dot{\gamma}, \qquad \text{and} \qquad [v_x]_{y=0} = 0.$$

It is interesting that the solution of Eqs. 4–6 and 22 gives same results, exhibiting the fact that the migration time to reach steady-state is much longer than the stress relaxation time. This flow history focuses on the transient response of shear banding systems following step shear rates, wherein it combines the usual start-up of flow and the step shear rate between two banded states along the stress plateau. The plots exhibit the formation of two velocity profiles of the banded flow and a jump across the interface in the polymeric stress. Initially, the first overshoot in the stress is

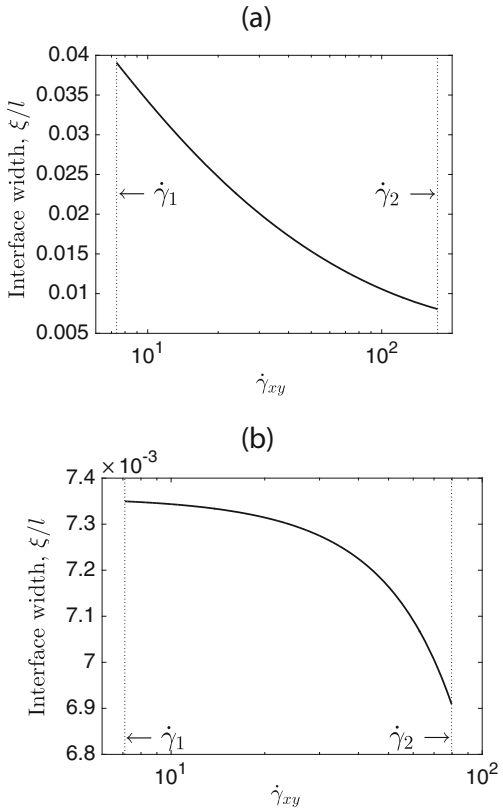

Fig. 10 Interface width as a function of applied shear rate for (**a**) a 5 wt. % CTAT wormlike micellar solution at 38 °C and (**b**) a 11 wt. % CTAB-$NaNO_3$ wormlike micellar solution at 28 °C

developed upon the inception of flow, and the second overshoot is produced by step shear rate along the stress plateau. The overshoot time scale is similar to that of the viscoelastic relaxation time. The fluidity profile, representative of fluid structure, reveals the regions of a more-structured fluid and less-structured fluid separated by an interface. The interface migration after the second change in shear rate (that occurring along the stress plateau) is depicted in Fig. 5d. Here, the interface separates two regions where the order parameter (the modified fluidity) is constant in space, and diffusion is negligible. This is predicted within the convective time scale.

In Fig. 6, an important observation is revealed: the minima in the spatial variation of the mechanical potential is preserved at the initial and the final end stages of the interface diffusion. This result derives from the fact that the diffusion occurs along the plateau stress where the spatial variation is given in Eq. 39. Accordingly, the interface achieves a constant value of $\pm\sqrt{u}$ as $y \rightarrow \pm\infty$ (Fig. 6d, upper curves, $\varphi^o(y)$), and hence the minima of the mechanical potential are located at the binodals of the plateau, where $\varphi^o = \pm\sqrt{u}$ (Fig. 6d, lower curves, $V(y)$). Notice that the spatial integration of Eq. 37 gives the equality of the mechanical potential with the first derivative of the spatial profile (39). Hence, in Fig. 6d, the mechanical potential curves are the derivatives of the $\varphi^o(y)$ profiles. In the case of the sharp interface (Fig. 5a–d), the derivative approaches a delta function in space, and consequently, $u \rightarrow 0$.

Observation of the velocity and structure profiles reveals that the structure does not show discontinuities in the same way that the velocity profile does. This is in accord with results by Helgeson et al. (2009).

Figure 7 shows the rheometric data and model predictions for the stress and first normal-stress difference for the CTAB/$NaNO_3$ solution. Agreement of predictions and data is excellent.

The migration of the interface to a new imposed shear rate starting from rest is illustrated in Fig. 8. Symbols are the results of the simulation for each shear rate and continuous lines follow a fitting procedure according to the expressions:

$$y_i(t) = \begin{cases} - \text{ (Absence of interface)} & \text{if } t < t_d \\ y_f + (1 - y_f)\exp\left[-\left(\frac{t-t_d}{\tau}\right)\right] & \text{if } t \geq t_d \end{cases}$$

As depicted in Fig. 8, a mono-exponential decay is approximately obtained. From these curves, a characteristic migration time τ_i is extracted from the fitting process and this is shown in a semi-log plot in Fig. 9 for various shear rates along the stress plateau. The migration time was calculated by two methods: the first one involves predictions of the displacement of the interfacial fluidity profile and the second one calculates the time of formation of the non-homogenous velocity profile. Differences in the migration time following the two methods are small. The migration time increases abruptly at small shear rates, followed by an exponential increase and a quasilinear relation at high shear rates. Indeed, the non-linear relationship of migration time with shear rate is a novel prediction of the model. Since the variation of the migration time with shear rate is non-linear, this indicates that the correlation length or the interface width may vary with the applied shear rate. Figure 8 shows that the position of the interface with time follows an exponential function, similarly as data on interface migration presented by Ballesta et al. (2007) using superposition rheology in shear banding systems.

Figure 9 further illustrates the position of the interface as a function of shear rate, revealing a linear relation that complies with the lever rule, a result that depicts agreement with data of Hu et al. (2008) and Helgeson et al. (2009).

Discussion

Elsewhere (Radulescu et al. 2003) the selection of the plateau stress in shear banding flows has been carried out by adding a stress diffusion term to the constitutive equations.

This criterion enables the discontinuous shear banding transition to be replaced by a smooth transition (over a length scale of order ξ), but the diffusion coefficient is not to what would be considered realistic. According to Renardy (2014), there are basically two assumptions underlying the idea of stress diffusion, i.e., particles diffuse according to Fick's law, stresses are determined by the moments of a single particle distribution function and that the mathematical consequences of stress diffusion are difficult to assess in general. The two first assumptions are quite reasonable for dumbbell models of dilute solutions, where the polymer molecules interact solely with solvent molecules. Stress diffusion resulting from Brownian forces acting on polymer molecules should be more complicated than Fick's law.

Birefringence data by Cappelaere et al. (1997) show clearly an advancing interface with increasing shear rate along the stress plateau. To model such behavior, here it is considered that the interface divides two regions of different refractive index or different order. We have identified these regions by a structural parameter which is the normalized fluidity, such as an increase in fluidity is related to a low-structured system and vice versa.

The calculated flow curve from the constitutive equations of the BMP model written in terms of the order parameter (the modified fluidity, Eq. 13) allows the calculation of the bifurcation parameter u, which is constant along the plateau stress. The extremes of the plateau (the binodals) correspond to the equal minima of the mechanical potential, from which the plateau stress is defined. It turns out that the areas above and below of the curve drawn of the product of the shear stress and shear rate (i.e., the dissipation) are equal.

Considering the reaction-diffusion G-L Eq. 23, its solution tends to a stable equilibrium value of the reaction process, namely, to a minimum of the mechanical potential. The effect of diffusion is to alter the rate of approach. If there are more than one local minima in the potential, then the solution will tend to the regions corresponding to the basin of attraction for the pure reaction equation (that without the diffusion term). In the neighborhood of the interface, the gradient of the fluidity is large, and diffusion is important. The description considered here is a boundary layer expansion, which involves the solution of Eq. 23 along the normal to the interface. This solution evolves into a traveling wave whose speed is proportional to the difference in the minima of the mechanical potential. The values of the minima in the mechanical potential are the asymptotic values of the fluidity in front and behind the interface, respectively. Following the motion of the front, it is possible to determine how the solution evolves in time.

An important result derives from the fact that the G-L equation provides a methodology to predict the interface diffusion if the mechanical potential of a cubic equation of state is known. Here the interface lies between bands of different flow structure, which can be measured by flow birefringence. If stress diffusion is sought, then the system of constitutive equations needs a diffusion term in the stress equation, which in addition to the structural diffusion, is known to produce spatial patterns (Turing patterns).

Regarding the stress diffusion coefficient, computations using the "diffusive" version of the Johnson-Segalman or Giesekus models, contrast with experimental data reported by Masselon et al. (2008). The "diffusive" version of the above models predicts that the time scale of the interface migration scales linearly with shear rate for all shear-banded states, implying a single value of the interface width. These predictions are not in agreement with data of the rapid exponential increase in the time scale with the applied shear rate, which incidentally, is predicted in Figs. 8 and 9. In Masselon et al. study (2008), a single strain diffusion coefficient is measured, which readily suggests that a possible dependence of the relaxation time on shear should be taken into account. This conclusion is clearly in accord with Eq. 5 or Eq. 44 of the BMP model, in which the relaxation time depends on structure. This particular behavior is not predicted by the "diffusive" version of the mentioned current models.

Data provided for the CTAT solution can be used to evaluate the variation of the interface thickness with shear rate. Given values of the diffusion coefficient $D' = 10^{-11}\mathrm{m}^2/\mathrm{s}$ (which is within the range of values reported by Fardin et al. 2015 and Mohammadigoushki and Muller 2016), $G_0 = 58$ Pa and $\varphi = 0.2\ \mathrm{Pa}^{-1}\mathrm{s}^{-1}$ (fluidity at the onset of the plateau, obtained from Fig. 3) gives an interface width of approximately 6 microns. At the end of the plateau, we have $\varphi = 5\ \mathrm{Pa}^{-1}\mathrm{s}^{-1}$, which gives a width of 1.3 microns. This yields a decrease of five times the interface width along the plateau stress. This decrease is in quantitative agreement with experimental observations of Fardin et al. (2015). Figure 10 shows the interface width as a function of the shear rate along the plateau.

It is important to mention that the model predictions exposed here agree with those shown elsewhere (Radulescu et al. 2003) where different time scales in the shear banding process of wormlike micelles are identified (band destabilization, reconstruction-sharpening and migration of the interface). Here, we identify the first process at short time scales as that produced by the existing "pitchfork" bifurcation, followed by the convective time scale (reconstruction and sharpening-flat profile) and migration (diffusion time scale). Following start-up of shear flow, the building of the banding structure starts with the relaxation of the stress overshoot, followed by the three stages for which at long times, the formation of a diffusive interface that migrates from the fixed wall to its stationary position in the gap is observed.

Finally, one notices that the structure of the G-L Eq. 24 is similar to those describing the "kink" migration or the dynamics of solitary waves. The similarities with these systems are exposed in the Appendix. It is tempting to suggest that the interface migrates as a soliton in time, or strictly speaking, as a solitary wave (Rajaraman 1987).

Conclusions

The steady-state version of the BMP model under shear flow written in terms of the modified fluidity (the order parameter) is a cubic equation from which a mechanical potential can be derived. The addition of a diffusion term in the equation for the fluidity (structural parameter) gives rise to the spatial profile of the interface between the two bands with different order. The interface width can be calculated according to Eq. 38. Given an input stress, the bifurcation parameters u and v can be calculated for every stress value, and thus the mechanical potential can be constructed. When $v = 0$, the mechanical potential possesses equal minima whose positions are functions of a single constant bifurcation parameter u, which corresponds to a plateau stress. The dissipation calculated along the plateau stress agrees with the equal-area rule. Concurrently, as a special case of the BMP equation, the G-L equation describes the interface migration through several time scales. The longest one corresponds to the diffusive one, with a displacement of the hyperbolic tangent profile with time. The derivative of such profile gives the potential with equal minima in the start and end of the interface migration. Since in the BMP model the stress relaxation time is structure-dependent, the diffusion coefficient of the interface is also structure-dependent, and hence, it is shear rate dependent. This dependency arises naturally from the formulation of the constitutive and conservation equations. Using data from experiments in wormlike solutions, predictions are in agreement with the reduction of interfacial width with shear rate.

Acknowledgements Financial support from CONACYT (National Council for Science and Technology) through project 235880 is acknowledged.

Appendix A: Similarities with the soliton equations

It is interesting that the expression for the free energy (41) is similar to that of the Landau mean field free energy of a flat interface and to the so-called φ^4-kink model. The potential shown in Fig. 2b is identical to that of the φ^4-kink model (Klein-Gordon model), which relies on the following expression for the free energy f:

$$f\left(\varphi^o\right) = \left(\varphi^o\right)^4/4 - u\left(\varphi^o\right)^2/2 \tag{50}$$

and therefore is the same as Eq. 16 with $v = 0$. The φ^4-kink model starts from Eq. 50 and produces the following equations for the order parameter and energy density, respectively:

$$\varphi^o(y) = \pm\sqrt{u}\tanh\left(\frac{y}{\sqrt{2}\xi}\right) \tag{51}$$

$$e(y) = \frac{1}{2}u^2\mathrm{sech}^4\left(\frac{y}{\sqrt{2}\xi}\right) \tag{52}$$

The energy density is strongly localized in space with a maximum in the center of the interface (or kink) and falling rapidly to zero for $y > \sqrt{2}\xi$. This result coincides to that of Eq. 38 (see Fig. 6d) where the order parameter profile and the potential are plotted with y.

Dynamics

The time-dependence of the kinks depend on the field $\varphi^o(y,t)$. A kinetic energy proportional to $(\partial\varphi^o/\partial t)^2$ is introduced so that the dynamic Hamiltonian associated with the free energy of Eq. 50 is:

$$H = \int dz\left[\frac{1}{2}\kappa_\varphi v_o^{-2}\left(\frac{\partial\varphi^o}{\partial t}\right)^2 + \frac{1}{2}\kappa_\varphi\left(\frac{\partial\varphi^o}{\partial y}\right)^2 + f\left(\varphi^o\right)\right] \tag{53}$$

where v_0 is a reference velocity and κ_φ/v_0^2 is analogous to the mass density in the Lagrangian elasticity theory. H should be interpreted as a Hamiltonian in which the first term of the integral is a momentum density. The equation of motion for $\varphi^o(y,t)$ is:

$$\frac{1}{v_0^2}\frac{\partial^2\varphi^o}{\partial t^2} + \frac{1}{\kappa_\varphi}\frac{\partial V}{\partial\varphi^o} - \frac{\partial^2\varphi^o}{\partial y^2} = 0 \tag{54}$$

Equations 53 and 54 are invariant under the Lorentz transformation. In particular, if the time-independent solution of Eq. 54 as $t \to \infty$ (38) is $\pm\sqrt{u}$, then the time-dependent solution is:

$$\varphi^o(y) = \pm\sqrt{u}\tanh\left(\frac{y-\omega t}{\sqrt{2}\xi'}\right) \tag{55}$$

$$\xi' = \sqrt{\kappa_\varphi\left(1-(\omega/v_0)^2\right)/u} \tag{56}$$

where ω is the interface velocity or kink velocity. There are special solutions to non-linear wave equations in which non-linearities and dispersion produce a wave packet whose shape is constant in time. Such constant shape solutions are called *solitary waves*. Equation 55, the dynamical kink solution is a solitary wave. Solutions in which well-separated solitary waves collide and emerge at large positive times with same shape as they have at times before the collision are generally called *solitons*. Strictly speaking, solitary waves are not in general solitons, unless the potential is harmonic.

Moreover, since the analysis exposed here concerns with wave equations where the order parameter is the fluidity representing two structures separated by the traveling interface or kink, experimentally this approach is consistent with the view of a traveling interface between birefringence bands. The process develops along the plateau stress, namely, a constant stress. Therefore, the fluidity times the stress is a shear rate, which implies that these birefringence bands and the interface between them can be associated with a shear wave.

Appendix B: modified BMP equation for Solitons

Consider an expression for the monotonic BMP equation plus a diffusion term as follows:

$$\frac{\partial \varphi}{\partial t} = a + b\varphi - c\varphi^2 + \kappa_\varphi \frac{\partial^2 \varphi}{\partial y^2} \tag{57}$$

The third-order mechanical potential V is given by:

$$V = \frac{1}{3}c\varphi^3 - \frac{1}{2}b\varphi^2 - a\varphi \tag{58}$$

So that Eq. 57 can be written as:

$$\frac{\partial \varphi}{\partial t} + V'(\varphi) = \kappa_\varphi \frac{\partial^2 \varphi}{\partial y^2} \tag{59}$$

It is well known that solitons and solitary waves are the class of special solutions of the Korteweg-de Vries (KdV) equation:

$$\frac{\partial \varphi}{\partial t} + \varphi \frac{\partial \varphi}{\partial y} + \beta \frac{\partial^3 \varphi}{\partial y^3} = 0 \tag{60}$$

This equation is an integrable Hamiltonian solved exactly by the inverse scattering transform, giving rise to a soliton solution. Solitons are localized traveling waves that have bell-shaped sech (φ) profile and tend asymptotically to zero at large distances. A particular soliton interacts with other solitons preserving its permanent form.

If a diffusion term is added, Eq. 60 is transformed into the so-called KdV- Burgers Equation (KdVB):

$$\frac{\partial \varphi}{\partial t} + \varphi \frac{\partial \varphi}{\partial y} - \alpha \frac{\partial^2 \varphi}{\partial y^2} + \beta \frac{\partial^3 \varphi}{\partial y^3} = 0 \tag{61}$$

wherein the Burgers equation is recovered as a special case ($\beta = 0$):

$$\frac{\partial \varphi}{\partial t} + \varphi \frac{\partial \varphi}{\partial y} - \alpha \frac{\partial^2 \varphi}{\partial y^2} = 0 \tag{62}$$

Notice that in Eq. 61 two limiting cases may be addressed: a dominant dissipation ($\alpha > \beta$) and a dominant dispersion ($\alpha < \beta$).

Applying the following transformation of a traveling wave:

$$\zeta = y - \omega t \tag{63}$$

Equation 61 becomes:

$$-\omega \frac{\partial \varphi}{\partial \zeta} + \varphi \frac{\partial \varphi}{\partial \zeta} - \alpha \frac{\partial^2 \varphi}{\partial \zeta^2} + \beta \frac{\partial^3 \varphi}{\partial \zeta^3} = 0 \tag{64}$$

The traveling wave solution, i.e. $\varphi = \varphi(\zeta)$ shall be considered here. The integration of Eq. 64 with respect to ζ yields the following non-linear differential equation:

$$\frac{\partial^2 \varphi}{\partial \zeta^2} - \frac{\alpha}{\beta}\frac{\partial \varphi}{\partial \zeta} - \frac{\omega}{\beta}\varphi + \frac{1}{2\beta}\varphi^2 = C \tag{65}$$

where C is an integration constant. Notice that this equation is similar to the traveling-wave transformed (57). If shear waves are considered in Eq. 57, an expression consistent with Eq. 62 is produced:

$$\frac{\partial \varphi}{\partial t} + \frac{\partial}{\partial y} V'(\varphi) = \kappa_\varphi \frac{\partial^2 \varphi}{\partial y^2} \tag{66}$$

or:

$$\frac{\partial \varphi}{\partial t} - b\frac{\partial \varphi}{\partial y} + 2c\varphi \frac{\partial \varphi}{\partial y} = \kappa_\varphi \frac{\partial^2 \varphi}{\partial y^2} \tag{67}$$

Applying the transformation (63) gives:

$$-\frac{\partial \varphi}{\partial \zeta}(v + b) + 2c\varphi \frac{\partial \varphi}{\partial \zeta} = \kappa_\varphi \frac{\partial^2 \varphi}{\partial \zeta^2} \tag{68}$$

Equation 68 is similar to Eq. 64 (with $\beta = 0$). If dispersion is included, then Eq. 66 should be generalized as follows:

$$\frac{\partial \varphi}{\partial t} + \frac{\partial}{\partial y} V'(\varphi) = \kappa_\varphi \frac{\partial^2 \varphi}{\partial y^2} - \beta \frac{\partial^3 \varphi}{\partial y^3} \tag{69}$$

Furthermore, in the case of a cubic equation of state,

$$V' = \varphi^3 - u\varphi \tag{70}$$

Equation 69 gives:

$$\frac{\partial \varphi}{\partial t} + 3\varphi^2 \frac{\partial \varphi}{\partial y} - u\frac{\partial \varphi}{\partial y} - \kappa_\varphi \frac{\partial^2 \varphi}{\partial y^2} + \beta \frac{\partial^3 \varphi}{\partial y^3} = 0 \tag{71}$$

Equation 71 is called the modified KdVB equation.

Discussion

Starting from the original BMP equation, namely,

$$\frac{\partial \varphi}{\partial t} = a + b\varphi - c\varphi^2 \tag{72}$$

Equation 72 can be expressed in terms of the mechanical potential as:

$$\frac{\partial \varphi}{\partial t} + V'(\varphi) = 0 \tag{73}$$

where

$$V = \frac{1}{3}c\varphi^3 - \frac{1}{2}b\varphi^2 - a\varphi \tag{74}$$

Overall, the general equation that includes dissipation and dispersion can be expressed as:

$$\frac{\partial \varphi}{\partial t} + \frac{\partial}{\partial y} V'(\varphi) - \kappa_\varphi \frac{\partial^2 \varphi}{\partial y^2} + \beta \frac{\partial^3 \varphi}{\partial y^3} = 0 \tag{75}$$

which contains the generalizations of the soliton solutions.

Equation 75 is the main result. It contains the two particular cases of dissipation dominated system ($\kappa_\varphi > \beta$) or the dispersion dominated system ($\kappa_\varphi < \beta$). Both situations depend on the derivatives of the mechanical potential V. Therefore, if the flow curve is monotonic or non-monotonic, there are situations where the soliton states form independently of the nature of the flow curve. In other terms, shear banding and shear waves can occur in monotonic or non-monotonic flow curves.

The constitutive equations consistent with these premises are then:

$$\begin{aligned} \frac{d\varphi}{dt} &= k_0 \left(1 + \vartheta \left(\sqrt{II_D}\right)\right)(\varphi_\infty - \varphi)\, \underline{\underline{\sigma}} : \underline{\underline{D}} \\ &\quad + \frac{1}{\lambda}(\varphi_0 - \varphi) + \kappa_\varphi \nabla^2 \varphi + \beta \nabla^2 |\nabla \varphi| \end{aligned} \tag{76}$$

$$\underline{\underline{\sigma}} + \tau_\sigma(\varphi) \overset{\nabla}{\underline{\underline{\sigma}}} = \frac{2}{\varphi} \underline{\underline{D}} \tag{77}$$

where the contributions from dissipation, diffusion and dispersion are explicitly exposed, although authors elsewhere consider the diffusion term part of the dissipative contribution.

Summarizing, Eq. 76 gives rise to a cubic flow curve or constitutive curve and to the modified-KdVB (71), whereas (76) with $\vartheta = 0$ gives rise to a monotonic constitutive curve and to the KdVB (Eq. 61).

References

Ballesta P, Lettinga MP, Manneville S (2007) Superposition rheology of shear-banding wormlike micelles. J Rheol 51(5):1047. doi:10.1122/1.2750665

Cappelaere E, Berret JF, Decruppe JP, Cressely R, Lindner P (1997) Rheology, birefringence, and small-angle neutron scattering in a charged micellar system: Evidence of a shear-induced phase transition. Phys Revx E 56(2):1869–1878. doi:10.1103/physreve.561869

Castillo HA, Castillo Tejas J, García-Sandoval JP, Matus O, Bautista F, Puig JE, Manero O (2014) Derivation of the mechanical and thermodynamic potentials from the generalized bmp model under shear-banding flow. J Non-Equilibrium Thermodyn 39(4):231–248. doi:10.1515/jnet-2014-0026

Fardin MA, Radulescu O, Morozov A, Cardoso O, Browaeys J, Lerouge S (2015) Stress diffusion in shear banding wormlike micelles. J Rheol 59(6):1335–1362. doi:10.1122/1.4930858

Frank RL, Hainzl C, Seiringer R, Solovej JP (2012) Microscopic derivation of Ginzburg-Landau theory. J Amer Math SocX 25(3):667–713. doi:10.1090/s0894-0347-2012-00735-8

García-Sandoval J, Manero O, Bautista F, Puig J (2012) Inhomogeneous flows and shear banding formation in micellar solutions: Predictions of the bmp model. J Non-Newtonian Fluid Mech 179:43–54. doi:10.1016/j.jnnfm.2012.05.006

Helgeson ME, Vasquez PA, Kaler EW, Wagner NJ (2009) Rheology and spatially resolved structure of cetyltrimethylammonium bromide wormlike micelles through the shear banding transition. J Rheol 53(3):727. doi:10.1122/1.3089579

Hu YT, Lips A (2005) Kinetics and mechanism of shear banding in an entangled micellar solution. J Rheol 49(5):1001. doi:10.1122/1.2008295

Hu YT, Palla C, Lips A (2008) Comparison between shear banding and shear thinning in entangled micellar solutions. J Rheol 52(2):379. doi:10.1122/1.2836937

Johnson M, Segalman D (1977) A model for viscoelastic fluid behavior which allows non-affine deformation. J Non-Newtonian Fluid Mech 2(3):255–270. doi:10.1016/0377-0257(77)80003-7

Lagarias JC, Reeds JA, Wright MH, Wright PE (1998) Convergence properties of the nelder-mead simplex method in low dimensions. SIAM J Optim 9(1):112–147

López-Barrón CR, Gurnon AK, Eberle APR, Porcar L, Wagner NJ (2014) Microstructural evolution of a model, shear-banding micellar solution during shear startup and cessation. Phys Rev E 89:042,301. doi:10.1103/PhysRevE.89.042301

Manero O, Pérez-López J, Escalante J, Puig J, Bautista F (2007) A thermodynamic approach to rheology of complex fluids: The generalized bmp model. J Non-Newtonian Fluid Mech 146(1-3):22–29. doi:10.1016/j.jnnfm.2007.02.012

Masselon C, Salmon JB, Colin A (2008) Nonlocal effects in flows of wormlike micellar solutions. Phys Rev Lett 100(3):038,301. doi:10.1103/physrevlett.100.038301

Mohammadigoushki H, Muller SJ (2016) A flow visualization and superposition rheology study of shear-banding wormlike micelle solutions. Soft Matter 12(4):1051–1061. doi:10.1039/c5sm02266e

Radulescu O, Olmsted PD, Decruppe JP, Lerouge S, Berret JF, Porte G (2003) Time scales in shear banding of wormlike micelles. Europhys Lett 62(2):230–236. doi:10.1209/epl/i2003-00351-x

Rajaraman R (1987) Solitons and instantons: An introduction to solitons and instantons in quantum field theory. Elsevier Science and Technology, Amsterdam

Renardy M (2014) Korteweg stresses and admissibility criteria for shear banded flows. J Non-Newtonian Fluid Mech 213:68–72. doi:10.1016/j.jnnfm.2014.09.012

Hosea ME, Shampine LF (1996) Analysis and implementation of TR-BDF2. Appl Numer Math 20(1–2):21–37. doi:10.1016/0168-9274(95)00115-8

Soltero JFA, Bautista F, Puig JE, Manero O (1999) Rheology of cetyltrimethylammonium p-toluenesulfonate-water system. 3. nonlinear viscoelasticity. Langmuir 15(5):1604–1612. doi:10.1021/la971299a

Van der Waals J (1895) Theorie thermodynamique de la capillarité dans l' hypothese d'une variation continué de densité. Arch Neerl Sci Exact Nat 28:121–209

Yuan XF (1999) Dynamics of a mechanical interface in shear-banded flow. Europhys Lett (EPL) 46(4):542–548